AERODYNAMIC CHARACTERIZATION OF A TYPICAL LAUNCH VEHICLE WITH TWO STRAPONS

C Babu[1], G Vidya[2], Dipankar Das[3], MM Patil[4], V Ashok[5]
Vikram Sarabhai Space Centre, Trivandrum-695022

ABSTRACT

Aerodynamics of a multi strapon launch vehicle is complex due to the presence of shocks, shock-boundary layer interactions and associated flow separation. The geometry is quite complex in the presence of various protuberances such as retro rockets, ullage rockets, wire tunnels, core-strapon attachments. In this paper, the results of CFD simulations carried out for a two strapon launch vehicle for several Mach numbers are summarized along with the comparison with wind tunnel test results in pitch plane. The validation exercise indicates that the CFD PARAS3D can be used for overall aerodynamic characterization within the dispersion bands specified.

Keywords: launch vehicle, CFD, validation, aerodynamic coefficients, angle of attack, Mach number.

INTRODUCTION

An expendable launch vehicle usually consists of an axisymmetric core with payload fairing of diameter same as core or a bulbous shape with two or four strapons attached at the aft for the purpose of augmentation of thrust. The core of the vehicle contains many protrusions or cylindrical structures

Which have functional purpose. Some of them are wire tunnels, destruct tunnels, retro and ullage rockets used during stage separation, etc. The strapons are attached to the core using near cylindrical attachments. The aerodynamic characterization of a typical launch vehicle has to be carried out in the entire Mach number regime ranging from subsonic, transonic and supersonic Mach numbers, where, strapon separation and stage separation usually occur at high altitude and low dynamic pressure conditions. In this paper, the aerodynamic characterization of a multi-body launch vehicle using in-house CFD code PARAS3D is presented along with validation with test data.

CONFIGURATION

Fig 1 shows the configuration under investigation. This launch vehicle consists of a core, two strapons and two sitvc tanks. The configuration contains numerous protuberances such as stringers, ullage and retro rockets, wire tunnels, destruct tunnel, core-strapon attachments, sitvc-core attachments, etc. The configuration is imported as CAD file (*stl* format) for CFD simulation and the configuration is scaled to 1:50 scale. The scaled model with the sting is shown in Figure 2

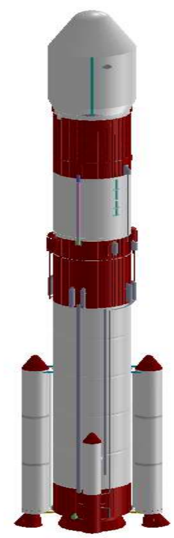

FIGURE 1: VIEW OF THE TWO STRAPON LAUNCH VEHICLE

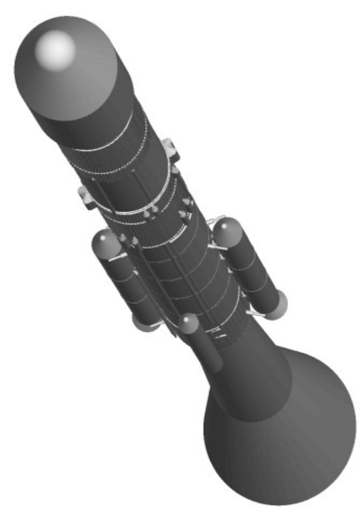

FIGURE 2: PERSPECTIVE VIEW OF THE CONFIGURATION WITH STING SIMULATED IN PARAS3D

DETAILS OF CFD SOLVER, GRID AND SIMULATION DETAILS:

1. PARAS 3D solves the 3D Reynolds Averaged Navier-Stokes (RANS) equations over Cartesian mesh using finite volume approach. The turbulence closure is through a high Reynolds number *k-ε* turbulence model and for the near the wall treatment wall function approach is used. The solver is capable of solution refinement based on the flow field gradients.

2. The free stream Mach number varies from M=0.8 to M=3.0 and the flow angle, angle of attack and angle of sideslip were fixed at 4 deg.

3. In upstream direction 50D is used and remaining sides 70D were kept to generate the initial grid. *Upwind* boundary condition is imposed on the upstream boundary. *Pressure/ Shift* boundary conditions are imposed in far field boundaries. The initial cell count is 36 million for all Mach numbers. The initial grid distribution, boundary conditions and the sign convention for angle of attack are shown in Figure 3. Angle of sideslip is positive if the flow direction is from –Z to +Z. Core and the two strapons face the flow when the angle of attack is positive; one sitvc tank is in the windward side and the other is in the leeward side. When angle of sideslip is positive, one strapon is in the windward side and the other strapon is in the leeward side and both the sitvc tanks face the flow in a similar way. A zoomed view of the initial grid distribution and final grid distribution in the symmetry plane is shown in Figure 4 for Mach number 0.8, α=4 deg. It may be observed that grid is refined in the area of flow gradients.

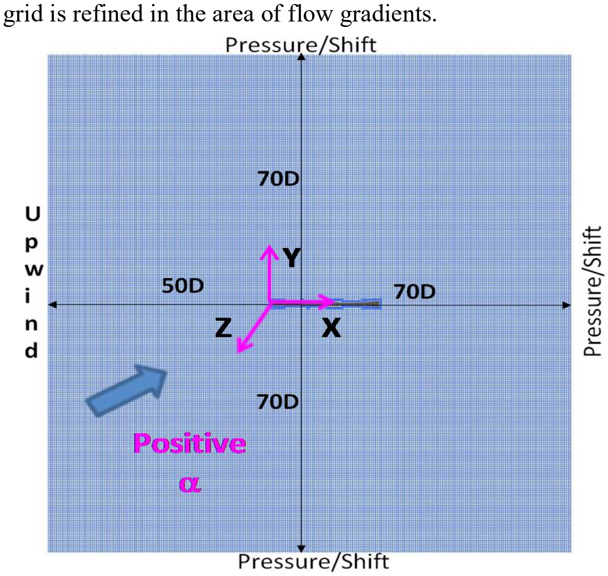

FIGURE 3: DOMAIN EXTENT, INITIAL GRID, BOUNDARY CONDITIONS AND SIGN CONVENTION

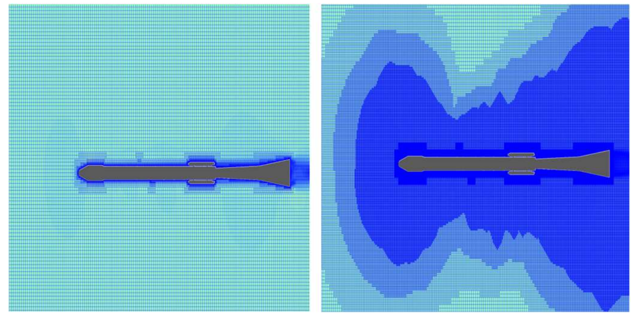

FIGURE 4: INITIAL GRID AND FINAL REFINED GRID IN THE SYMMETRY PLANE AT M=0.8 AND 4 DEG ANGLE OF ATTACK

Initial grid cell count is 36 million. Three times grid refinement was carried out based on flow gradients for all Mach numbers. The final grid size if from 70 million to 140 million after third refinement. Grid independence and convergence of normal force coefficient at M=0.8 and 1.2 with α=4 deg are shown in Figure 5. It is observed that the normal force coefficient matches for the last two refined grids. The % change between the results for the force (axial, normal) and moment (pitching moment) coefficients are shown in Figure 6 for all Mach numbers. It can be noticed that it is generally within 2%.

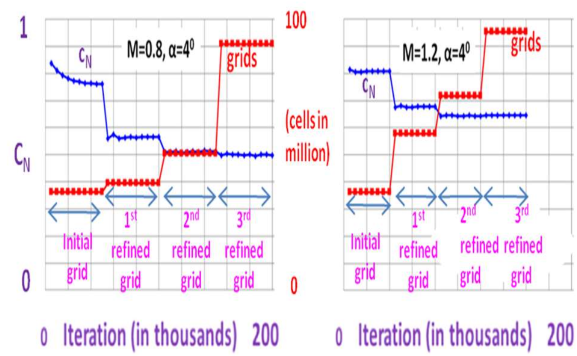

FIGURE 5: GRID INDEPENDENCE AND CONVERGENCE OF NORMAL FORCE COEFFICIENT AT M=0.8 AND 1.2 WITH α=4 DEG

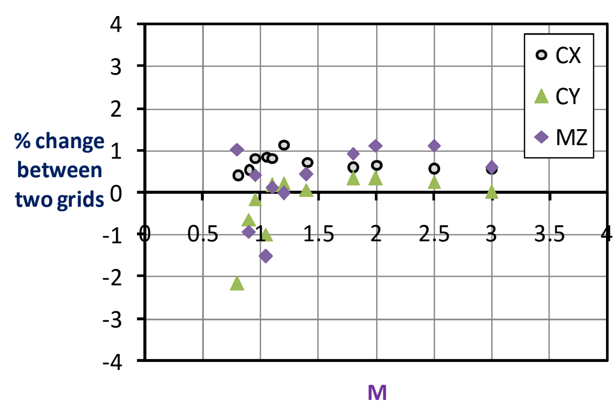

FIGURE 6: GRID INDEPENDENCE AND CONVERGENCE OF FORCE AND MOMENT COEFFICIENTS AT α=4 DEG

RESULTS AND DISCUSSION

Mach palette in the vehicle symmetry plane (Z=0) is shown in Fig. 7. The supersonic pocket of flow over the PLF (Payload Fairing) at M=0.8 is clearly evident. The wake behind the SITVC tanks is indicated by a low Mach number zone. The shock is detached at M=1.2 and moves closer to the nose at M=2.0. The deceleration of the flow aft of nose shock and the flow expansion in the cylinder and aft of boat tail at M=1.2 as well as M=2.0 are visible. The shocks created due to the strapon nose and SITVC nose are also visible in the Mach palette.

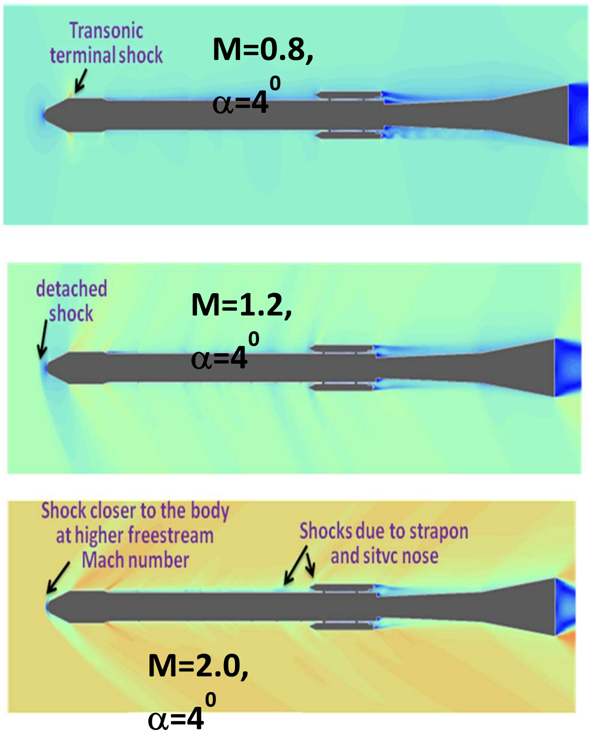

FIGURE 7: MACH NUMBER PALETTE IN THE SYMMETRY PLANE AT SELECT MACH NUMBERS AND 4 DEG ANGLE OF ATTACK

Cp distribution over the configuration (perspective views) at select Mach numbers, M=0.8, 1.2 and 2.0 are shown in Figure 8. It can be observed that stagnation Cp increases when Mach number increases from M=0.8 to M=2.0. This is observed in PLF, strapon and SITVC tank nose cap region. The pressure jumps due to the various protrusions over core cylinder, core-strapon and core-sitvc attachments are clearly evident.

The distribution of the cumulative axial force coefficient along the length of the vehicle is depicted in Figure 9. Only the pressure drag coefficient is plotted here. The forebody extent is identified in the figure. Further increase in drag coefficient is due to the core and strapon base region. It is observed that the fore body drag coefficient is the minimum at M=0.8 and maximum at M=1.2. Drag coefficient falls with further increase in Mach number from M=1.2.

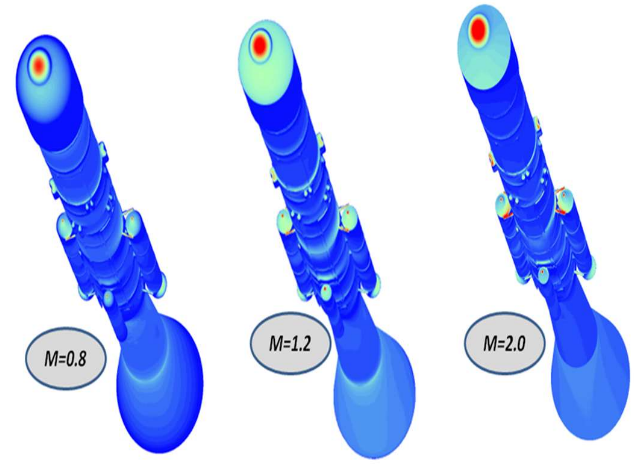

FIGURE 8: CP DISTRIBUTION OVER THE COMPLETE VEHICLE AT SELECT MACH NUMBERS AT 4 DEG ANGLE OF ATTACK

Skin friction drag coefficient is computed using in-house software based on empirical methods (***CDROC***) and is added to the CFD based pressure drag coefficient in the forebody (marked in Figure 9). This estimate is compared with the wind tunnel test results for forebody axial force coefficient and shown in Figure 10. It can be noted that the prediction is within ±8%, transonic Mach numbers are lower predicted and higher predicted at supersonic Mach numbers

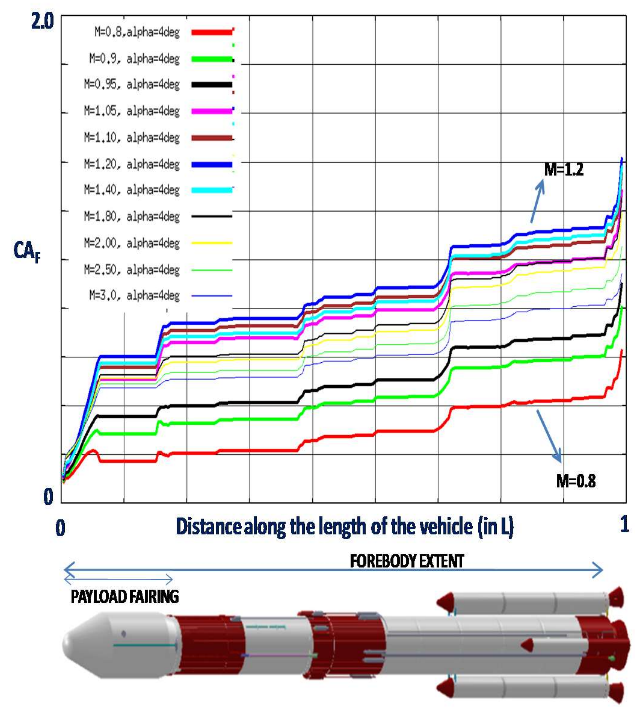

Figure 9: CUMULATIVE FORE BODY AXIAL FORCE COEFFICIENT ALONG THE VEHICLE LENGTH AT ALL MACH NUMBERS.

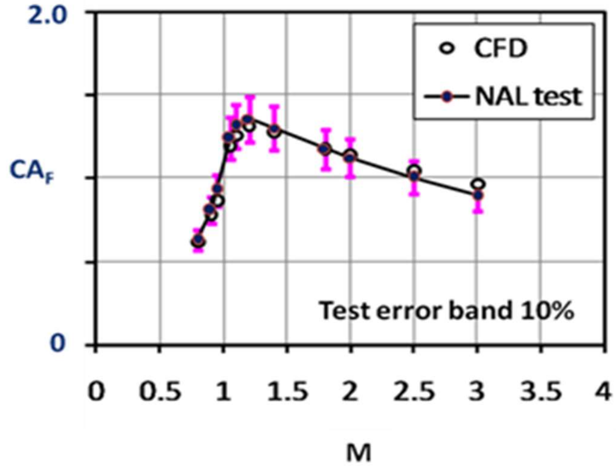

FIGURE 10: COMPARISON OF CFD RESULTS WITH WIND TUNNEL TEST DATA: FORE BODY AXIAL FORCE COEFFICIENT.

The distribution of cumulative normal force coefficient slope with distance in the axial direction from nose to base is depicted in Figure 11. The load increases along the nose cone for all Mach numbers, except for transonic Mach numbers in PLF cylinder region due to shock-boundary layer interactions. The flow is also separated in the boat tail region for transonic Mach numbers whereas the flow is attached at high supersonic Mach numbers. The load continues to increase in the core cylinder due to the presence of stringers, protrusions and wire tunnels for all Mach numbers. The sudden rise in load at ~65% of the length of the configuration is due to the strapon nose cone related load and its interference effect on the core. The interference due to the SITVC tanks is felt as a drop in load (due to the placement with respect to the flow angle), followed by rise in load again in the cylindrical region. The load up to the strapon region is ~40% of the total load in the transonic Mach numbers, whereas it rises to ~50% in the high supersonic Mach numbers. The vehicle normal force coefficient distribution is the lowest at M=0.8 and peaks at M=1.8. The load at higher Mach numbers are close to the value at M=1.8.

The normal force coefficient slope computed by CFD is compared with the wind tunnel test results and shown in Figure 12. It can be noted that the prediction, is in general, more by 4% to 10%, except at M=0.8 where it is less by 6%.

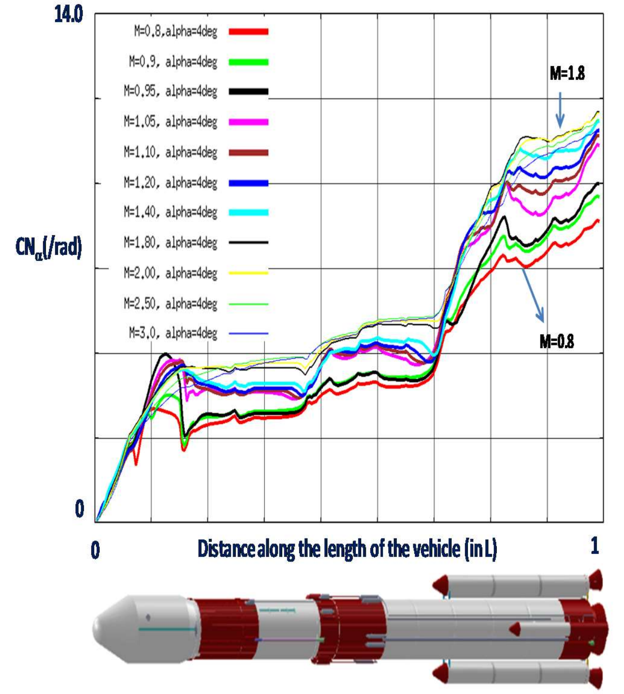

FIGURE 11: CUMULATIVE NORMAL FORCE COEFFICIENT SLOPE ALONG THE VEHICLE LENGTH AT ALL MACH NUMBERS.

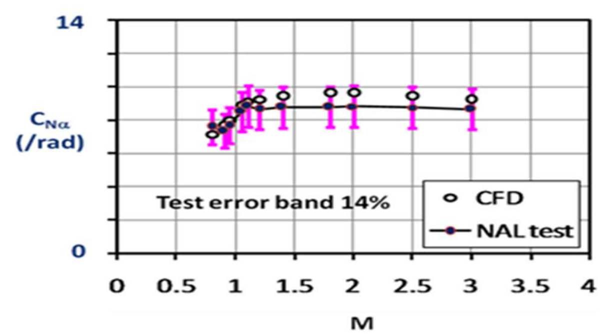

FIGURE 12: COMPARISON OF CFD RESULTS WITH WIND TUNNEL TEST DATA NORMAL FORCE COEFFICIENT SLOPE.

The development of center of pressure with distance in the axial direction from nose to base is depicted in Figure 13. The trend of center of pressure almost correlates with cumulative normal force coefficient distribution as seen in Figure 11. The sudden rise in center of pressure aft of ~65% of the length of the configuration is due to the strapon nose cone related load and its interference effect on the core as well the destructive interference due to the SITVC tanks. The center of pressure peaks at transonic Mach number 0.95 due to the relatively larger aft body contribution to load. The center of pressure shifts forward with increase in Mach number due to reduced interference loads and the domination of load over core cylinder region.

CFD computed center of pressure is compared with the wind tunnel test results and shown in Figure 14. It can be noted that the prediction, is within ±1.6%L

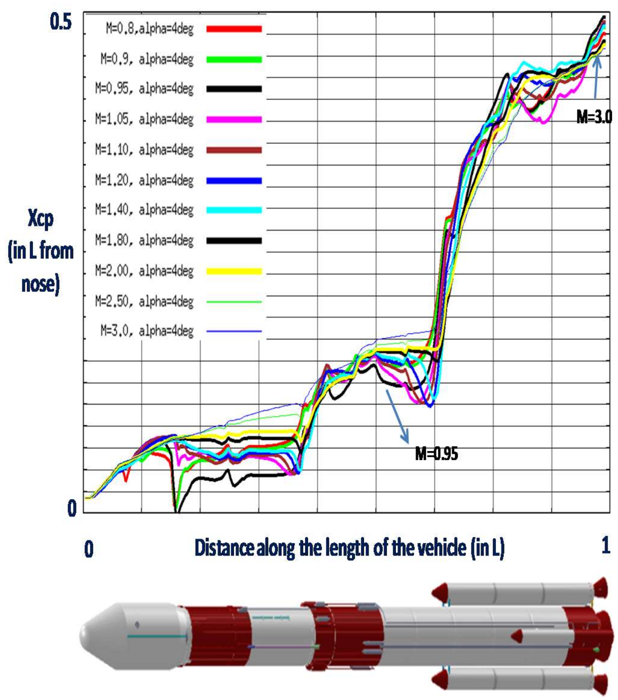

FIGURE 13: CUMULATIVE CENTRE OF PRESSURE ALONG THE VEHICLE LENGTH AT ALL MACH NUMBERS

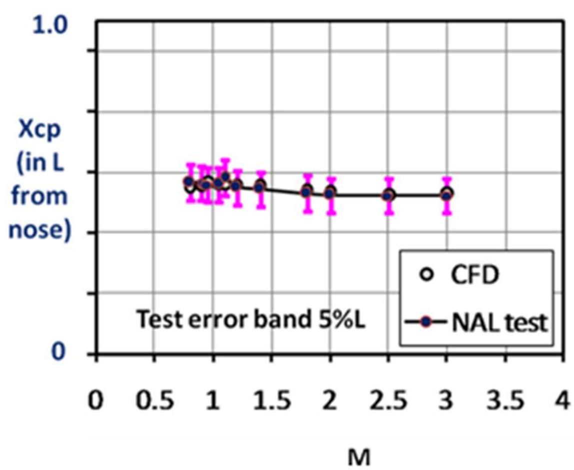

FIGURE 14: COMPARISON OF CFD RESULTS WITH WIND TUNNEL TEST DATA: CENTRE OF PRESSURE

CONCLUSION

PARAS3D RANS solver is one of the main aerodynamic design and data generation tool used in VSSC. It uses the Cartesian grid and solution refinement based on the flow field gradients to study various configurations during design stage. In this paper, aerodynamic coefficients are computed using PARAS3D in pitch plane of the typical launch vehicle and the comparison with wind tunnel measurement is made. In general PARAS 3D, captures the trend and magnitude of CA_F, $CN\alpha$ and XCp which matches closely with wind tunnel measurement. Axial force coefficient compares within ±8% as compared to measurement results. The predicted $CN\alpha$ is lower in subsonic Mach number and higher in supersonic Mach number as compared to wind tunnel measurement. Centre of pressure compares well with in ±1.6%L as compared to wind tunnel measurement. The CFD results are within the dispersion specified by wind tunnel measurement.